Parameters of cosmological models and recent astronomical observations

G. S. Sharov[1] and E. G. Vorontsova[1]

[1] *Tver state university*
*170002, Sadovyj per. 35, Tver, Russia**

For different gravitational models we consider limitations on their parameters coming from recent observational data for type Ia supernovae, baryon acoustic oscillations, and from 34 data points for the Hubble parameter $H(z)$ depending on redshift. We calculate parameters of 3 models describing accelerated expansion of the universe: the ΛCDM model, the model with generalized Chaplygin gas (GCG) and the multidimensional model of I. Pahwa, D. Choudhury and T.R. Seshadri. In particular, for the ΛCDM model 1σ estimates of parameters are: $H_0 = 70.262\pm0.319\,\mathrm{km\,c^{-1}Mpc^{-1}}$, $\Omega_m = 0.276^{+0.009}_{-0.008}$, $\Omega_\Lambda = 0.769\pm0.029$, $\Omega_k = -0.045 \pm 0.032$. The GCG model under restriction $\alpha \geq 0$ is reduced to the ΛCDM model. Predictions of the multidimensional model essentially depend on 3 data points for $H(z)$ with $z \geq 2.3$.

arXiv:1407.5405v1 [gr-qc] 21 Jul 2014

I. INTRODUCTION

The most important challenge for cosmologists is to explain the accelerated expansion of our universe that was directly measured for the first time from Type Ia supernovae observations [1, 2]. These supernovae were used as standard candles, because one can measure their redshifts z and luminosity distances D_L. The observed dependence $D_L(z)$ based on further measurements [3, 4] argues for the accelerated growth of the cosmological scale factor $a(t)$ at late stage of its evolution.

This result was confirmed via observations of cosmic microwave background anisotropy [5], baryon acoustic oscillations (BAO) or large-scale galaxy clustering [4, 6, 7] and other observations [4, 5, 8]. In particular, our attention should be paid to measurements of the Hubble parameter $H(z)$ for different redshifts z [9–20]. The results of these measurements and estimations are represented below in Table VI of Appendix.

The values $H(z)$ were calculated with two methods: evaluation of the age difference for galaxies with close redshifts in Refs. [9–15] and the method with BAO analysis [16–20].

In the first method the equality

$$a(t) = a_0/(1+z) \tag{1}$$

and its consequence

$$H(z) = \frac{1}{a(t)}\frac{da}{dt} = -\frac{1}{1+z}\frac{dz}{dt}$$

are used. Here $a_0 \equiv a(t_0)$ is the current value of the scale factor a.

Baryon acoustic oscillations (BAO) are disturbances in the cosmic microwave angular power spectrum and in the correlation function of the galaxy distribution, connected with acoustic waves propagation before the recombination epoch [4, 6]. These waves involved baryons coupled with photons up to the end of the drag era corresponding to $z_d \simeq 1059.3$ [8], when baryons became decoupled and resulted in a peak in the galaxy-galaxy correlation function at the comoving sound horizon scale $r_s(z_d)$ [6, 8].

*Electronic address: german.sharov@mail.ru

In Table V of Appendix we represent estimations of two observational manifestations of the BAO effect. These values are taken from Refs. [5, 21, 22], they confirm the conclusion about accelerated expansion of the universe. In addition, this data with observations of Type Ia supernovae and the Hubble parameter $H(z)$ are stringent restrictions on possible cosmological theories and models.

To explain accelerated expansion of the universe various cosmological models have been suggested, they include different forms of dark matter and dark energy in equations of state and various modifications of Einstein gravity [23–25]. The most popular among cosmological models is the ΛCDM model with a Λ term (dark energy) and cold dark matter (see reviews [23, 25]). This model with 5% fraction of visible baryonic matter nowadays ($\Omega_b = 0.05$), 24% fraction of dark matter ($\Omega_c = 0.24$) and 71% fraction of dark energy ($\Omega_\Lambda = 0.71$) [5] successfully describes observational data for Type Ia supernovae, anisotropy of cosmic microwave background, BAO effects and $H(z)$ estimates [4, 5, 8].

However, there are some problems in the ΛCDM model connected with vague nature of dark matter and dark energy, with fine tuning of the observed value of Λ, which is many orders of magnitude smaller than expected vacuum energy density, and with surprising proximity Ω_Λ and $\Omega_m = \Omega_b+\Omega_c$ nowadays, though these parameters depend on time in different ways (the coincidence problem) [23–26].

Therefore a large number of alternative cosmological models have been proposed. They include modified gravity with $f(R)$ Lagrangian [27, 28], theories with scalar fields [29, 30], models with nontrivial equations of state [31–39], with extra dimensions [40–47] and many others [23–26].

Among these gravitational models we concentrate here on the model with generalized Chaplygin gas (GCG) [31–37]. The equation of state in this model

$$p = -B_0/\rho^\alpha \tag{2}$$

generalizes the corresponding equation $p = -B/\rho$ for the original Chaplygin gas model [31]. Generalized Chaplygin gas with EoS (2) plays the roles of both dark matter and dark energy, it is applied to describing observations of type Ia supernovae, BAO effects, the Hubble parameter $H(z)$ and other observational data in various combinations [33–37].

The equation of state similar to Eq. (2) is used in the multidimensional gravitational model of I. Pahwa, D. Choudhury and T.R. Seshadri [46] (the PCS model in references below). In this model the $1 + 3 + d$ dimensional spacetime is symmetric and isotropic in two subspaces: in 3 usual spatial dimensions and in d additional dimensions. Matter has zero (dust-like) pressure in usual dimensions and negative pressure p_e in the form (2) in extra dimensions:

$$T^\mu_\nu = \mathrm{diag}\,(-\rho, 0, 0, 0, p_e, \dots, p_e), \qquad p_e = -B_0\rho^{-\alpha} \tag{3}$$

(in Sects. I, II we use units with $c = 1$).

In Ref. [46] the important case $d = 1$ was omitted. This case was considered in Ref. [47], where we analyzed singularities of cosmological solutions in the PCS model [46] and suggested how to modify the equation of state (3) for the sake of avoiding the finite-time future singularity ("the end of the world") which is inevitable in the PCS model. Main advantages of the multidimensional models [46] and [47] are: naturally arising dynamical compactification and successful description of the Type Ia supernovae observations.

In this paper we compare the ΛCDM model, the model with generalized Chaplygin gas (GCG) [31, 32], and also the models PCS [46] and [47] with d extra dimensions from the point of view of their capacity to describe recent observational data for type Ia supernovae, BAO and $H(z)$. In the next section we briefly summarize the dynamics of the mentioned models, in Sect. III we analyze parameters of the mentioned models resulting in the best description of the observational data from Ref. [3] and Appendix.

II. MODELS

For all cosmological models in this paper the Einstein equations

$$G^\mu_\nu = 8\pi G T^\mu_\nu + \Lambda\delta^\mu_\nu, \tag{4}$$

determine dynamics of the universe. Here T^μ_ν and $G^\mu_\nu = R^\mu_\nu - \frac{1}{2}R\delta^\mu_\nu$ are the energy momentum tensor and the Einstein tensor, Λ is nonzero only in the ΛCDM model. The energy momentum tensor has the form (3) in the multidimensional models [46, 47] and the standard form

$$T^\mu_\nu = \mathrm{diag}\,(-\rho, p, p, p) \tag{5}$$

in models with 3+1 dimensions. In the ΛCDM model baryonic and dark matter may be considered as one component of dust-like matter with density $\rho = \rho_b + \rho_{dm}$, so we suppose $p = 0$ in Eq. (5). The fraction of relativistic matter (radiation and neutrinos) is close to zero for observable values $z \le 2.3$. In the GCG model [31–37] pressure p in the form (2) plays the role of dark energy, corresponding to the Λ term in the ΛCDM model.

For the Robertson-Walker metric with the curvature sign k

$$ds^2 = -dt^2 + a^2(t)\Big[(1-kr^2)^{-1}dr^2 + r^2 d\Omega\Big] \tag{6}$$

the Einstein equations (4) are reduced to the system

$$3\frac{\dot a^2 + k}{a^2} = 8\pi G\rho + \Lambda, \tag{7}$$

$$\dot\rho = -3\frac{\dot a}{a}(\rho + p). \tag{8}$$

Eq. (8) results from the continuity condition $T^\mu_{\nu;\mu} = 0$, the dot denotes the time derivative.

Using the present time values of the Hubble constant and the critical density

$$H_0 = \frac{\dot a}{a}\Big|_{t=t_0} = H\Big|_{z=0}, \qquad \rho_{cr} = \frac{3H_0^2}{8\pi G}, \tag{9}$$

we introduce dimensionless time τ, densities $\bar\rho_i$, pressure $\bar p$ and logarithm of the scale factor [46, 47]:

$$\tau = H_0 t, \qquad \bar\rho = \frac{\rho}{\rho_{cr}}, \qquad \bar\rho_b = \frac{\rho_b}{\rho_{cr}}, \qquad \bar p = \frac{p}{\rho_{cr}}, \qquad \mathcal{A} = \log\frac{a}{a_0}. \tag{10}$$

We denote derivatives with respect to τ as primes and rewrite the system (7), (8)

$$\mathcal{A}'(\tau) = \sqrt{\bar\rho + \Omega_\Lambda + \Omega_k e^{-2\mathcal{A}}}, \tag{11}$$

$$\bar\rho'(\tau) = -3\mathcal{A}'(\bar\rho + \bar p). \tag{12}$$

Here

$$\Omega_m = \frac{\rho(t_0)}{\rho_{cr}}, \qquad \Omega_\Lambda = \frac{\Lambda}{3H_0^2}, \qquad \Omega_k = -\frac{k}{a_0^2 H_0^2} \tag{13}$$

are present time fractions of matter ($\Omega_m = \Omega_b + \Omega_c$), dark energy and curvature in the equality

$$\Omega_m + \Omega_\Lambda + \Omega_k = 1, \tag{14}$$

resulting from Eq. (7) if we fix $t = t_0$.

If we know an equation of state $\bar{p} = \bar{p}(\bar{\rho})$ for any model, we can solve the Cauchy problem for the system (11), (12) including initial conditions for variables (10) at the present epoch $t = t_0$ (here and below $t = t_0$ corresponds to $\tau = 1$)

$$\mathcal{A}\big|_{\tau=1} = 0, \qquad \bar{\rho}\big|_{\tau=1} = \Omega_m. \tag{15}$$

In the ΛCDM model Eq. (12) yields $\bar{\rho} = \Omega_m e^{-3\mathcal{A}} = \Omega_m(1+z)^3$, so we solve only equation (11)

$$\mathcal{A}'^2 = \frac{H^2}{H_0^2} = \Omega_m e^{-3\mathcal{A}} + \Omega_\Lambda + \Omega_k e^{-2\mathcal{A}}. \tag{16}$$

with the first initial condition (15).

Equation (12) may be solved also and in the GCG model, but in this case we are to decompose all matter into two components [34–38]. One of these components is usual dust-like matter including baryonic matter; the other component is generalized Chaplygin gas with density $\rho_g \equiv \rho_{GCG}$ (and corresponding $\bar{\rho}_g = \rho_g/\rho_{cr}$). If the first component is pure baryonic and the latter describes both dark matter and dark energy, equations of state are:

$$\bar{\rho} = \bar{\rho}_b + \bar{\rho}_g, \qquad \bar{p}_b = 0, \qquad \bar{p} = \bar{p}_g = -B\,(\bar{\rho}_g)^{-\alpha} \tag{17}$$

If we use the integrals $\bar{\rho}_b = \Omega_b e^{-3\mathcal{A}}$ and $\bar{\rho}_g = \big[B + Ce^{-3\mathcal{A}(1+\alpha)}\big]^{1/(1+\alpha)}$ of Eq. (12) for these components, equation (11) takes the form [33–38]

$$\mathcal{A}'^2 = \frac{H^2}{H_0^2} = \Omega_b e^{-3\mathcal{A}} + (1-\Omega_b-\Omega_k)\Big[B_s + (1-B_s)\,e^{-3\mathcal{A}(1+\alpha)}\Big]^{1/(1+\alpha)} + \Omega_k e^{-2\mathcal{A}}. \tag{18}$$

We solve this equation with the initial condition (15) $\mathcal{A}\big|_{\tau=1} = 0$. The dimensionless constant B_s [37, 38] (it is denoted A_s in Refs. [34, 35]) is expressed via B or B_0:

$$B_s = B\cdot(1-\Omega_b-\Omega_k)^{-1-\alpha}, \qquad B = B_0\,\rho_{cr}^{-1-\alpha}. \tag{19}$$

For the multidimensional model PCS [46] and the model [47] in spacetime with $1+3+d$ dimensions the following metric is used [46]:

$$ds^2 = -dt^2 + a^2(t)\left(\frac{dr^2}{1-kr^2} + r^2 d\Omega\right) + b^2(t)\left(\frac{dR^2}{1-k_2R^2} + R^2 d\Omega_{d-1}\right). \tag{20}$$

Here $b(t)$ and k_2 are the scale factor and curvature sign in extra dimensions (along with a and k for usual dimensions). For cosmological solutions in Refs. [46, 47] the scale factor $a(t)$ grows while $b(t)$ diminishes, in other words, some form of dynamical compactification [40–46] takes place, a size of compactified b is small enough to play no essential role at the TeV scale.

In Refs. [46, 47] the authors considered only one component of their matter. Here we generalize these models and introduce the "usual" component with density $\bar{\rho}_b$ and the "exotic" component with $\bar{\rho}_e = \rho_e/\rho_{cr}$ and pressure $\bar{p}_e = p_e/\rho_{cr}$ in extra dimensions similarly to Eq. (17):

$$\bar{\rho} = \bar{\rho}_b + \bar{\rho}_e, \qquad \bar{p}_e = -B\,(\bar{\rho}_e)^{-\alpha} \tag{21}$$

Dynamical equations for the models [46, 47] result from the Einstein equations (5) with $\Lambda = 0$ and the energy momentum tensor (3), (21). In our notation (10) with $\mathcal{B} = \log(b/b_0)$ (where $b_0 = b(t_0)$) these equations for $k_2 = 0$ and $d > 1$ are [46, 47]

$$\mathcal{A}'' = \frac{1}{d+2}\Big[d(d-1)\,\mathcal{B}'(\tfrac{1}{2}\mathcal{B}' - \mathcal{A}') - 3(d+1)\,\mathcal{A}'^2 - 3d\bar{p}_e + (2d+1)\Omega_k e^{-2\mathcal{A}}\Big], \tag{22}$$

$$\bar{\rho}_b' = -\bar{\rho}_b(3\mathcal{A}' + d\mathcal{B}'), \qquad \bar{\rho}_e' = -3\bar{\rho}_e\mathcal{A}' - d(\bar{\rho}_e + \bar{p}_e)\,\mathcal{B}', \tag{23}$$

$$\mathcal{B}' = (d-1)^{-1}\Big[-3\mathcal{A}' + \sqrt{3[(d+2)\,\mathcal{A}'^2 + 2(d-1)\,(\bar{\rho} + \Omega_k e^{-2\mathcal{A}})]/d}\Big]. \tag{24}$$

If $d = 1$ one should use [47]

$$\mathcal{B}' = (\bar{\rho} + \Omega_k e^{-2\mathcal{A}})/\mathcal{A}' - \mathcal{A}' \tag{25}$$

instead of Eq. (24).

For the system (22) – (23) the initial conditions include Eqs. (15) and the additional condition

$$\mathcal{A}'|_{\tau=1} = 1 \tag{26}$$

resulting from definitions of $\mathcal{A}$ (10) and H_0 (9):

$$\mathcal{A}'(\tau) = \frac{d}{d\tau}\log\frac{a}{a_0} = \frac{1}{H_0}\frac{\dot{a}}{a}.$$

For the model PCS [46, 47] we have the analog of Eq. (14)

$$\Omega_m + \Omega_B + \Omega_k = 1, \tag{27}$$

resulting from Eqs. (24) or (25) at $\tau = 1$. Here $\Omega_B = -d(B' + \frac{d-1}{6}B'^2)|_{\tau=1}$ is the contribution from d extra dimensions.

The models ΛCDM, GCG, PCS with suitable values of model parameters have cosmological solutions describing accelerated expansion of the universe [5, 8, 33–37, 46, 47]. We consider restrictions on these parameters coming from recent observational data for type Ia supernovae [3], BAO [5, 21, 22] and from measuring the Hubble parameter $H(z)$ [9–20], (Tables V, VI).

III. OBSERVATIONAL DATA AND MODEL PARAMETERS

Recent observational data on Type Ia supernovae in the Union2.1 compilation [3] include redshifts $z = z_i$ and distance moduli μ_i with errors σ_i for $N_S = 580$ supernovae. The distance modulus $\mu_i = \mu(D_L) = 5\log(D_L/10\text{pc})$ is logarithm of the luminosity distance [8, 23]:

$$D_L(z) = \frac{c\,(1+z)}{H_0\sqrt{|\Omega_k|}}\,\mathrm{Sin}_k\bigg(H_0\sqrt{|\Omega_k|}\int\limits_0^z\frac{d\tilde{z}}{H(\tilde{z})}\bigg), \qquad \mathrm{Sin}_k(x) = \begin{cases}\sinh x, & \Omega_k > 0,\\ x, & \Omega_k = 0,\\ \sin x, & \Omega_k < 0.\end{cases} \tag{28}$$

In particular, for the flat universe ($k = \Omega_k = 0$) the expression (28) is

$$D_L = c\,(1+z)\int\limits_0^z\frac{d\tilde{z}}{H(\tilde{z})} = \frac{ca_0^2}{H_0 a(\tau)}\int\limits_\tau^1\frac{d\tilde{\tau}}{a(\tilde{\tau})},$$

To describe the Type Ia supernovae data [3] we fix values of model parameters $p_1, p_2, \dots$ for the chosen model ΛCDM, GCG or PCS and calculate dependence of the scale factor $a(\tau)$ on dimensionless time τ. Further, we calculate numerically the integral expression (28) and the distance modulus $\mu(\tau)$. For each value of redshift z_i in the table [3] we find the corresponding $\tau = \tau_i$ with using linear approximation in Eq. (1) and the theoretical value $\mu_{th} = \mu(\tau_i, p_1, p_2, \dots)$ from the dependence $\mu(\tau)$ (28).

We search a good fit between theoretical predictions μ_{th} and the observed data μ_i as the minimum of

$$\chi^2_S(p_1, p_2, \dots) = \sum_{i=1}^{N_S}\frac{[\mu_i - \mu_{th}(z_i, p_1, p_2, \dots)]^2}{\sigma_i^2} \tag{29}$$

or the maximum of the corresponding likelihood function $\mathcal{L}_S(p_1,p_2,\ldots)=\exp(-\chi^2_S/2)$ in the space of model parameters $p_1,p_2,\ldots$

The Type Ia supernovae data [3] and the best fits for the mentioned models ΛCDM, GCG and PCS are shown in Fig. 1b in z, D_L plane. Details of the optimization procedure are described below.

Model predictions for the Hubble parameter $H(z)=\dot a/a=H_0\mathcal{A}'(\tau)$ we compare with observational data [9–20], from Table VI (Fig. 1c) and use the χ^2 function similar to (29):

$$\chi^2_H(p_1,p_2,\ldots)=\sum_{i=1}^{N_H}\frac{[H_i-H_{th}(z_i,p_1,p_2,\ldots)]^2}{\sigma^2_{H,i}}. \tag{30}$$

Here $N_H=34$, theoretical values $H_{th}(z_i,\ldots)=H_0\mathcal{A}'(\tau(z_i))$ are obtained from the calculated dependence $\mathcal{A}(\tau)$ and the equality (1) $z=e^{-\mathcal{A}}-1$.

The observational data for BAO [5, 21, 22] (Table V) includes two measured values [6]

$$d_z(z)=\frac{r_s(z_d)}{D_V(z)} \tag{31}$$

and

$$A(z)=\frac{H_0\sqrt{\Omega_m}}{cz}D_V(z). \tag{32}$$

They are connected with the distance [5, 6, 8]

$$D_V(z)=\biggl[\frac{czD_L^2(z)}{(1+z)^2H(z)}\biggr]^{1/3}, \tag{33}$$

expressed here via the luminosity distance (28).

The BAO observations [5, 21, 22] in Table V are not independent. So the χ^2 function for the values (31) and (32)

$$\chi^2_B(p_1,p_2,\ldots)=(\Delta d)^TC_d^{-1}\Delta d+(\Delta A)^TC_A^{-1}\Delta A. \tag{34}$$

includes the columns $\Delta d=[d_{z,th}(z_i,p_1,\ldots)-d_z(z_i)]$, $\Delta A=[A_{th}(z_i,p_1,p_2,\ldots)-A(z_i)]$, $i=1,\ldots,N_B$ and the covariance matrices C_d^{-1} and C_A^{-1} [5, 21] described in Appendix.

The best fits to the observational data for Type Ia supernovae [3], $H(z)$ and BAO data from Tables V, VI are presented in Fig. 1 for the models ΛCDM, GCG and PCS (with $d=1$ and $d=6$). The values of model parameters are tabulated below in Table II. They are optimal from the standpoint of minimizing the sum of all χ^2 (29), (30) and (34):

$$\chi^2_\Sigma=\chi^2_S+\chi^2_H+\chi^2_B. \tag{35}$$

Predictions of different models in Fig. 1 are rather close, in particular, the curves for the models ΛCDM and GCG practically coincide. The Hubble parameter $H(z)$ in Fig. 1c is measured in km c^{-1}Mpc^{-1}, the distances $D_L(z)$ and $D_V(z)$ in Fig. 1b, d are in Gpc.

The data points for $D_V(z)=r_s(z_d)/d_z(z)$ in Fig. 1d are calculated from $d_z(z_i)$ in Table V. Here the error boxes include the data spread between the recent estimations of the comoving sound horizon size:

$$r_s(z_d)=147.49\pm0.59\ \text{Mpc [8]},\qquad r_s(z_d)=153.3\pm2.0\ \text{Mpc [17, 21]}. \tag{36}$$

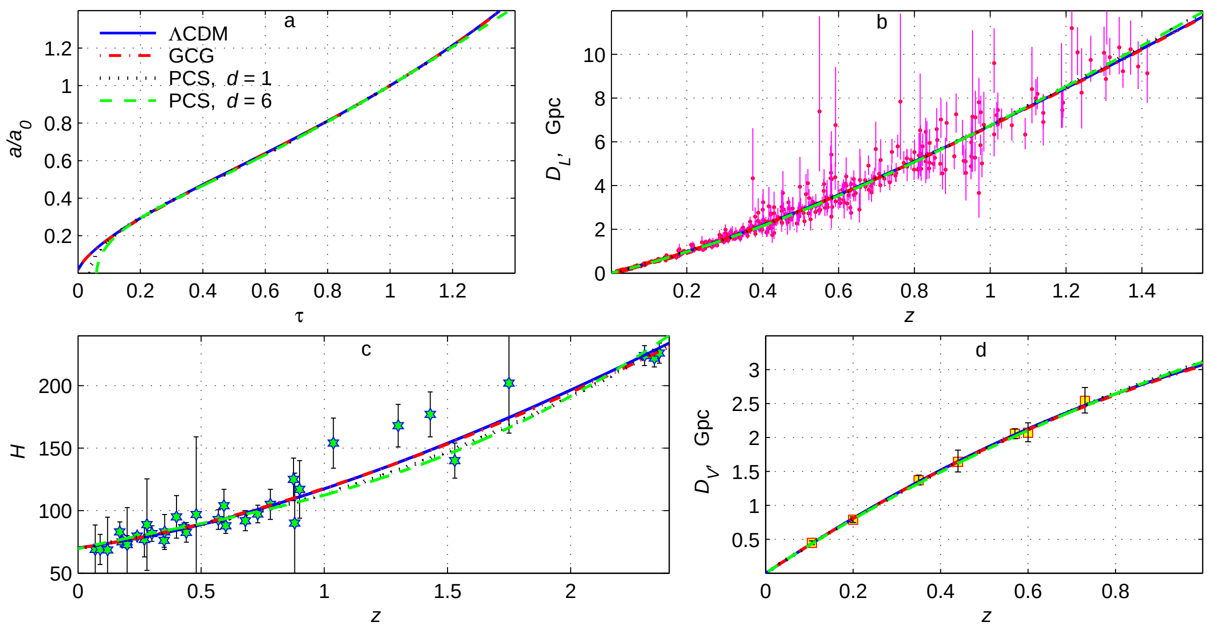

FIG. 1: For the models ΛCDM, GCG, PCS ($d = 1$ and $d = 6$) with the optimal values of model parameters from Table II we present (a) the scale factor $a(\tau)$; (b) the luminosity distance $D_L(z)$ and the Type Ia supernovae data [3]; (c) dependence $H(z)$ with the data points from Table VI and (d) the distance (33) $D_V(z)$ with the data points from Table V.

A. ΛCDM model

In the ΛCDM model we use three free parameters H_0, Ω_m and Ω_Λ in Eq. (16) for describing the considered observational data at $z \le 2.3$. For the Hubble constant H_0 different approaches result in different estimations. In particular, observations of Cepheid variables in the project Hubble Space Telescope (HST) give the recent estimate $H_0 = 73.8 \pm 2.4$ km c^{-1}Mpc^{-1} [48]. On the other hand, the satellite projects Planck Collaboration (Planck) [8] and Wilkinson Microwave Anisotropy Probe (WMAP) [5] for observations of cosmic microwave background anisotropy result in the following values (in km c^{-1}Mpc^{-1}):

$$\begin{array}{ll} H_0 = 67.3 \pm 1.2 & \text{(Planck [8])}, \\ H_0 = 69.7 \pm 2.4 & \text{(WMAP [5])}, \\ H_0 = 73.8 \pm 2.4 & \text{(HST [48])}. \end{array} \tag{37}$$

The nine-year results from WMAP [5] include also the estimate $H_0 = 69.33 \pm 0.88$ km c^{-1}Mpc^{-1} with added recent BAO and H_0 observations.

For the ΛCDM model many authors [5, 8, 49–55] calculated the best fits for parameters H_0, Ω_m and Ω_Λ for describing the Type Ia supernovae, $H(z)$ and BAO data in various combinations. In Refs. [52–55] some other cosmological models were compared with the ΛCDM model. In particular, the authors [52] compared 8 models with two information criteria including minimal χ^2 and the number of model parameters. Optimal values of these parameters were pointed out in Ref. [52] with the exception of H_0, though H_0 is the important parameter for all 8 models.

In Refs. [53–55] the ΛCDM, XCDM and ϕCDM models were applied to describe the supernovae, $H(z)$ and BAO data. For all mentioned models the authors [53–55] fixed two values of the Hubble constant $H_0 = 68 \pm 2.8$ [56] and $H_0 = 73.8 \pm 2.4$ km c^{-1}Mpc^{-1} [48] and searched optimal values of other model parameters. But they did not estimated the best choice of H_0 among these two values and in the segment between them.

In this paper we pay the special attention to dependence of χ^2_Σ minima on H_0. This dependence is very important if we compare different cosmological models.

The results of calculations [5, 8, 51–55], as usual, are presented as level lines for the functions $\chi^2(p_1, p_2)$ or $\mathcal{L}_S(p_1, p_2) = \exp(-\chi^2_S/2)$ of two parameters at 1σ (68.27%), 2σ (95.45%) and 3σ (99.73%) confidence levels. In particular, if a value H_0 is fixed, these two parameters for the ΛCDM model may be Ω_m and Ω_Λ.

In Fig. 2 we use this scheme for 3 fixed values H_0 (37) indicated on the panels (including the optimal value $H_0 = 70.262$ km c^{-1}Mpc^{-1}) and draw level lines of the functions (29), (30), (34) and (35) $\chi^2(\Omega_m, \Omega_\Lambda)$ in the Ω_m, Ω_Λ plane and for $\chi^2_\Sigma(\Omega_m, H_0)$ with fixed $\Omega_\Lambda = 0.769$ in the bottom-right panel. The points of minima are marked in Fig. 2 as hexagrams for χ^2_S, pentagrams for χ^2_H, diamonds for χ^2_B and circles for χ^2_Σ. Minimal values of the functions χ^2 (29), (30), (34) and (35) at these points are tabulated in Table I so we can compare efficiency of this description for different H_0. For the same purpose we point out the corresponding values χ^2 for some level lines in Fig. 2 and present the dependence of minima $\min \chi^2_\Sigma$ on H_0 and on Ω_m in the left bottom panels of Fig. 2. Here we denote $\min \chi^2_\Sigma(H_0) = \min\limits_{\Omega_m,\Omega_\Lambda} \chi^2_\Sigma$, $\min \chi^2_\Sigma(\Omega_m) = \min\limits_{H_0,\Omega_\Lambda} \chi^2_\Sigma$ and graphs of the fractions χ^2_S, χ^2_H, χ^2_B in $\min \chi^2_\Sigma(H_0)$ are also shown.

In the bottom panels we present how parameters of a minimum point of χ^2_Σ depend on H_0 and on Ω_m. In particular, for the dependence on H_0 the coordinates $\Omega_m(H_0)$ and $\Omega_\Lambda(H_0)$ of this point are calculated, the value Ω_k is determined from Eq. (14). For the dependence on Ω_m we also present the graph $h(\Omega_m)$, where $h = H_0/100$.

We see in Fig. 2 and in Table I that the dependence of $\min \chi^2_\Sigma(H_0)$ is appreciable and significant. This function has the distinct minimum and achieves its minimal value 585.35 at $H_0 \simeq 70.26$. The optimal values of the ΛCDM model parameters $\Omega_m \simeq 0.276$, $\Omega_\Lambda \simeq 0.769$, corresponding to this minimum are presented in Table II, these values are taken for the ΛCDM curves in Fig. 1.

The mentioned sharp dependence of $\min \chi^2_\Sigma$ on H_0 is connected with two factors: (1) the similar dependence of the main contribution $\chi^2_S(H_0)$ shown in the same panel; (2) the large shift of the minimum point for χ^2_S in the Ω_m, Ω_Λ plane corresponding to H_0 growth. For $H_0 = 68$ and 73.8 km c^{-1}Mpc^{-1} this minimum point is far from the similar points of χ^2_H and χ^2_B. Only for H_0 close to 70 km c^{-1}Mpc^{-1} all these three minimum points are near each other (the top-right panel in Fig. 2).

Only the value $H_0 = 69.7$ km c^{-1}Mpc^{-1} in Table I is close to the optimal value in Table II. We may conclude that the values of the Hubble constant $H_0 = 68$ and 73.8 km c^{-1}Mpc^{-1} taken in Refs. [53–55], unfortunately, lie to the left and to the right from the optimal value $H_0 \simeq 70$ km c^{-1}Mpc^{-1}. We see the significant difference between the large values $\min \chi^2_\Sigma = 673.64$ or 707.84 for the too small and too large values of H_0 in Table I and the optimal value $\min \chi^2_\Sigma = 585.35$ for $H_0 = 70.262$ in Table II.

In the middle row panels of Fig. 2 with χ^2_Σ the flatness line $\Omega_m + \Omega_\Lambda = 1$ (or $\Omega_k = 0$) is shown as the black dashed straight line. This line shows that only for H_0 close to the optimal value from Table II the following recent observational limitations on the ΛCDM model parameters (13) from surveys [5, 8]

$$\text{WMAP [5]:}\quad \begin{array}{l} \Omega_m = 0.279 \pm 0.025, \\ \Omega_\Lambda = 0.721 \pm 0.025, \\ \Omega_k = -0.0027^{+0.0039}_{-0.0038}; \end{array} \qquad \text{Planck [8]:}\quad \begin{array}{l} \Omega_m = 0.314 \pm 0.02 \\ \Omega_\Lambda = 0.686 \pm 0.025, \\ \Omega_k = -0.0005^{+0.0065}_{-0.0066} \end{array} \tag{38}$$

are satisfied on 1σ or 2σ level. For $H_0 = 67.3$ and 73.8 km c^{-1}Mpc^{-1} the optimal values of parameters Ω_m, Ω_Λ, Ω_k in Table I are far from restrictions (38) for Ω_k even on 3σ level.

Graphs of the optimal values Ω_m, Ω_Λ and Ω_k depending on H_0 are presented in the second bottom panel. We see that the value Ω_m weakly depends on H_0, but Ω_Λ and Ω_k satisfy conditions

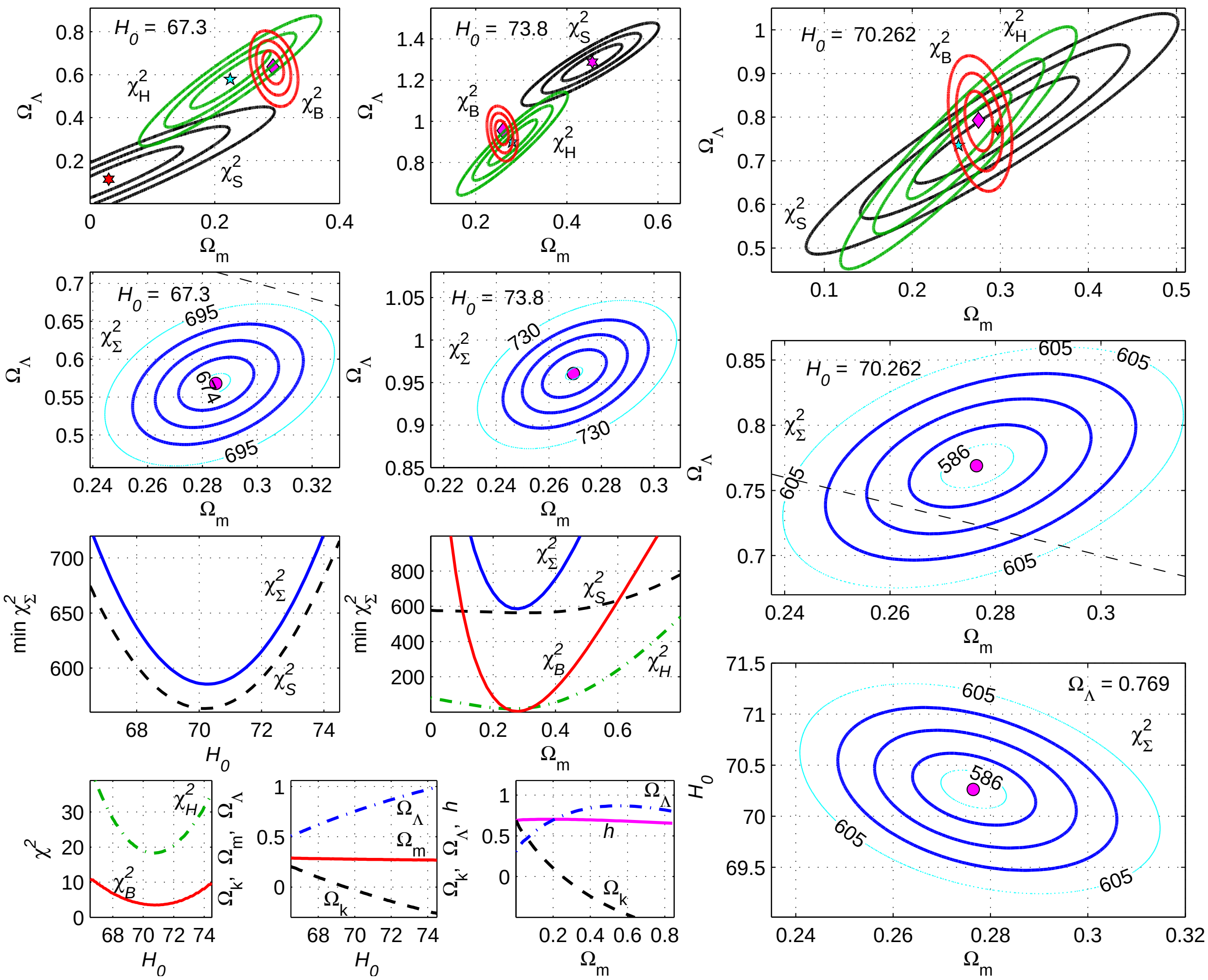

FIG. 2: The ΛCDM model. For the values H_0 (37) and the optimal value $H_0 = 70.26\ \mathrm{km\,c^{-1}Mpc^{-1}}$ level lines are drawn at 1σ, 2σ and 3σ (thick solid) for $\chi^2_S(\Omega_m, \Omega_\Lambda)$ (black), for $\chi^2_H(\Omega_m, \Omega_\Lambda)$ (green) and $\chi^2_B(\Omega_m, \Omega_\Lambda)$ (red in the top row), the sum (35) $\chi^2_\Sigma(\Omega_m, \Omega_\Lambda)$ (the middle row), $\chi^2_\Sigma(\Omega_m, H_0)$ for $\Omega_\Lambda = 0.758$ (the bottom-right panel); dependence of $\min \chi^2_\Sigma$, its fractions χ^2 and parameters of a minimum point on H_0 and on Ω_m.

TABLE I: The ΛCDM model. For given H_0 (37) the calculated minima of χ^2_S, χ^2_H, χ^2_B and χ^2_Σ with Ω_m, Ω_Λ, Ω_k correspondent to $\min \chi^2_\Sigma$.

H_0	$\min \chi^2_S$	$\min \chi^2_H$	$\min \chi^2_B$	$\min \chi^2_\Sigma$	Ω_m	Ω_Λ	Ω_k
67.3	599.37	18.492	5.548	673.64	0.285	0.568	0.147
69.7	562.73	17.993	3.517	588.53	0.278	0.734	−0.012
73.8	639.90	19.466	5.322	707.84	0.269	0.961	−0.230

(38) only for $H_0 \simeq 70\ \mathrm{km\,c^{-1}Mpc^{-1}}$.

The dependence of $\min\limits_{H_0,\Omega_\Lambda} \chi^2_\Sigma$ on Ω_m is rather sharp because of the correspondent dependence of its fraction χ^2_B. This fact for χ^2_B is connected with the contribution from the value $A(z)$ (32) measurements, because $A(z)$ is proportional to $\sqrt{\Omega_m}$ and χ^2_B is very sensitive to Ω_m values. Note that the fractions χ^2_S and χ^2_H (in $\min \chi^2_\Sigma$) weakly depend on Ω_m.

Dependencies of $\min \chi^2_\Sigma$ on H_0, Ω_m and also Ω_Λ, Ω_k let us calculate estimates of acceptable values for these model parameters. They are presented below in Table III.

Coordinates $h = H_0/100$ and Ω_Λ of the minimum point for χ^2_Σ depend on Ω_m in a such manner that only for $\Omega_m \simeq 0.27$ values Ω_Λ and Ω_k satisfy conditions (38). Note that the optimal value of h is close to 0.7 for all Ω_m in the limits $0 < \Omega_m < 1$.

B. GCG model

Let us apply the model with generalized Chaplygin gas (GCG) [31–37] to describing the same observational data for Type Ia supernovae, $H(z)$ and BAO. We use here Eq. (18) with the initial condition $\mathcal{A}|_{\tau=1} = 0$, so we have 5 independent free parameters in this model: H_0, Ω_b, Ω_k, α and B_s. However we really used only 4 free parameters, because the fraction Ω_b may include not only baryonic but also a part of cold dark matter. Our calculations yield that the minimum over remaining 4 parameters $\min\limits_{H_0,\Omega_k,\alpha,B_s} \chi^2_\Sigma$ practically does not depend on Ω_b in the range $0 \le \Omega_b \le 0.25$ (see Fig. 3). So in our analysis presented in Fig. 3 (except for 3 bottom-right panels) we fixed the value

$$\Omega_b = 0.047,$$

that is the simple average of the WMAP $\Omega_b = 0.0464$ [5] and Planck $\Omega_b = 0.0485$ [8] estimations.

In the GCG model $\Omega_\Lambda = 0$ and $\Omega_m = 1 - \Omega_k$ in accordance with Eq. (14) and the formal definition (13). However we should use the effective value Ω_m^{eff} in this model, in particular, in expression (32). In Refs. [34–38] the following effective value is used

$$\Omega_m^{eff} = \Omega_b + (1 - \Omega_b - \Omega_k)(1 - B_s)^{1/(1+\alpha)}. \tag{39}$$

This value results from correspondence between the models ΛCDM with Eq. (16) and GCG with Eq. (18) in the early universe at $z \gg 1$.

But in our investigation the majority of observational data is connected with redshifts $0 < z < 1$, so in Eq. (32) we are to consider the present time limit of the value $\Omega_m^{eff} \equiv \Omega_{0m}^{eff} = \lim\limits_{z\to 0} \Omega_m^{eff}$. If we compare limits of the right hand sides of Eqs. (16) and (18) at $z \to 0$ or $\mathcal{A} \to 0$, we obtain another effective value

$$\Omega_m^{eff} = \Omega_b + (1 - \Omega_b - \Omega_k)(1 - B_s). \tag{40}$$

Values χ^2_B calculated with expressions (39) and (40) are different if $\alpha \neq 0$. This difference looks like rather small if we compare minima of the sum (35) $\min \chi^2_\Sigma = \min\limits_{\Omega_k,\alpha,B_s} \chi^2_\Sigma$ depending on H_0. In Fig. 3 this dependence with Eq. (40) for Ω_m^{eff} is the blue solid line and for the case with Eq. (39) it is the violet dash-and-dot line. We see that the lines closely converge in the vicinity of the minimum point $H_0 \simeq 70$ km c^{-1}Mpc^{-1}. The dependence $\min \chi^2_\Sigma(H_0)$ in both cases (39) and (40) has the sharp minimum and resembles the case of the ΛCDM model in Fig. 2. The value $\min \chi^2_\Sigma \simeq 584.54$ of this minimum, its parameters in Table II, graph of the contribution χ^2_S and dependence on H_0 for parameters α, Ω_k, B_s of the minimum point in the bottom-left panel in Fig. 3 are presented for the case with Eq. (40).

One should note that all mentioned dependencies are different for the case (39), in particular, the absolute minimum of χ^2_Σ is 584.31. This difference is illustrated in the central panels in Fig. 3 with level lines of $\chi^2_\Sigma(\alpha, B_s)$ for $H_0 = 73.8$ and 70.093 km c^{-1}Mpc^{-1} (with the specified values Ω_k, optimal for these H_0). These level lines are blue for the expression (40) and they are thin violet for Eq. (39). Positions of the optimal points are close only if H_0 is close to its optimal value in Table II.

We suppose that the estimation of χ^2_B with the expression (40) is more adequate to the considered values z. So in Table II and in other panels of Fig. 3 we use only Eq. (40). Notations in Fig. 3 correspond to Fig. 2.

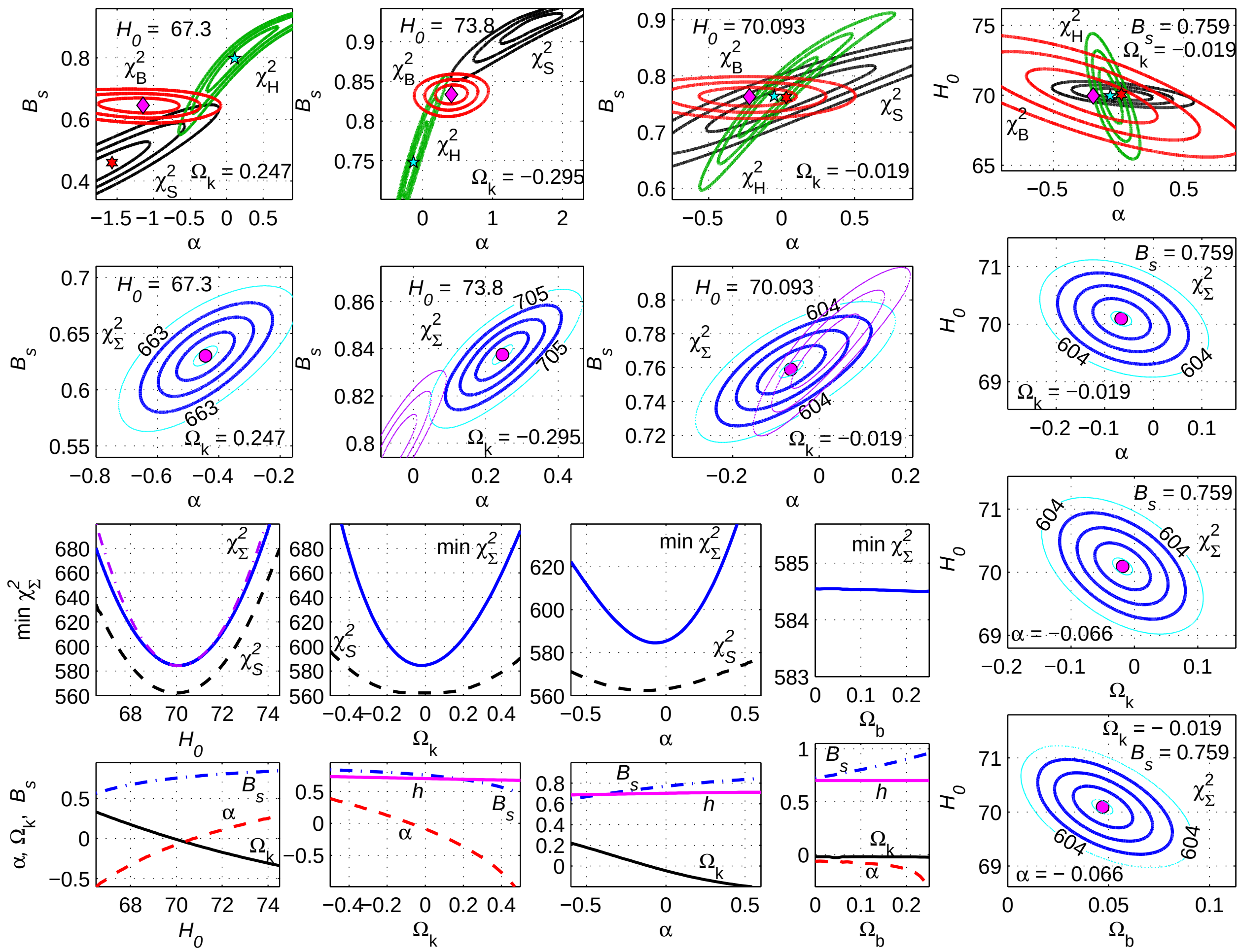

FIG. 3: The GCG model. For H_0 (37) and the optimal value $H_0 = 70.093\ \mathrm{km\,c^{-1}Mpc^{-1}}$ level lines of χ^2_Σ and other χ^2 are presented in α, B_s; α, H_0; Ω_k, H_0 and Ω_b, H_0 planes in notations of Fig. 2. In the bottom-left panels we analyze dependence of $\min\chi^2_\Sigma$ and parameters of a minimum point on H_0, Ω_k, α and Ω_b.

The similar dependence of $\min\chi^2_\Sigma$ on H_0 for the ΛCDM and GCG models results in unsuccessful description of the data with $H_0 = 67.3$ and $73.8\ \mathrm{km\,c^{-1}Mpc^{-1}}$ with the corresponding optimal values $\Omega_k = 0.247$ and -0.295. Fig. 3 illustrates large distances between minimum points of χ^2_S, χ^2_H and χ^2_B in these cases. The mentioned distances are small for the optimal values from Table II $H_0 = 70.093\ \mathrm{km\,c^{-1}Mpc^{-1}}$ and $\Omega_k = -0.19$. For these optimal values we present level lines of χ^2_Σ in α, B_s; α, H_0; Ω_k, H_0 and Ω_b, H_0 planes. In these panels other model parameters are fixed and specified.

When we test dependence of the minimum $\min\chi^2_\Sigma$ on H_0, Ω_k, α and Ω_b in Fig. 3, we minimize this value over all other parameters (except for the above mentioned Ω_b). In particular, $\min\chi^2_\Sigma(\Omega_k) = \min\limits_{H_0,\alpha,B_s}\chi^2_\Sigma$, this function has the distinct minimum near $\Omega_k \simeq 0$ and resembles the dependence $\min\chi^2_\Sigma(H_0)$. The optimal value of H_0 or $h = H_0/100$ is practically constant and close to $h \simeq 0.7$ if we vary Ω_k, α or Ω_b. As mentioned above the dependence of $\min\chi^2_\Sigma$ on Ω_b is very weak, so we fixed in our previous analysis $\Omega_b = 0.047$.

For the graph $\min\chi^2_\Sigma(\alpha) = \min\limits_{H_0,\Omega_k,B_s}\chi^2_\Sigma$ the correspondent minimum is achieved if α is negative: $\alpha = -0.066$ (see Table II). In the GCG model this parameter is connected with the square of adiabatic sound speed [33, 36, 37]

$$c_s^2 = \frac{\delta p}{\delta \rho} = -\alpha\frac{p}{\rho}. \tag{41}$$

If we accept the restriction $\alpha \geq 0$ (equivalent to $c_s^2 \geq 0$) in our investigation with the mentioned observational data, we obtain the optimal value $\alpha = 0$ and the GCG model will be reduced to the ΛCDM model with $\Omega_\Lambda = B = B_s(1-\Omega_b-\Omega_k)$. The dependence of $\min\chi^2_\Sigma$ and other parameters on α in Fig. 3 show that for $\alpha = 0$ we have $\min\chi^2_\Sigma \simeq 585.35$ and the optimal values of H_0, Ω_k, $\Omega_\Lambda = B$ corresponding to the ΛCDM model in Table II.

TABLE II: Optimal values of model parameters ($\Omega_b = 0.047$, for the GCG model $\Omega_m = \Omega_m^{eff}$ (40)).

Model	$\min\chi^2_\Sigma$	H_0	Ω_m	other parameters
ΛCDM	585.35	70.262	0.276	$\Omega_\Lambda = 0.769$, $\Omega_k = -0.045$
GCG	584.54	70.093	0.277	$\Omega_k = -0.019$, $\alpha = -0.066$, $B_s = 0.759$
PCS, $d = 1$	588.41	69.52	0.286	$\Omega_k = -0.040$, $\alpha = -0.256$, $B = 2.067$
PCS, $d = 2$	591.10	69.49	0.288	$\Omega_k = -0.017$, $\alpha = -0.372$, $B = 1.599$
PCS, $d = 3$	592.18	69.34	0.288	$\Omega_k = -0.027$, $\alpha = -0.431$, $B = 1.461$
PCS, $d = 6$	592.56	69.29	0.289	$\Omega_k = -0.029$, $\alpha = -0.493$, $B = 1.302$

C. PCS model

The multidimensional gravitational model of I. Pahwa, D. Choudhury and T.R. Seshadri [46] has the set of model parameters H_0, Ω_b, Ω_m, Ω_k, α, B similar to the GCG model, but also it has the additional integer-valued parameter d (the number of extra dimensions). Our analysis demonstrated that the value $d = 1$ is the most preferable for describing the observational data for supernovae, BAO and $H(z)$.

So it is the case $d = 1$ that we present in almost all panels of Fig. 4 (except for 2 panels with dependencies of $\min\chi^2_\Sigma$ on H_0 and Ω_k). We use the similarity of model parameters for the GCG and PCS models draw in Fig. 4 the same graphs and level lines for the PCS model as in Fig. 3 in correspondent panels. Colors of correspondent lines also coincide. Naturally we use in Fig. 4 the value B instead of B_s.

The minimum $\min\chi^2_\Sigma$ (over all other parameters) increases when the baryon fraction Ω_b grows. This dependence is more distinct than in the GCG case (Fig. 3), but it is also rather weak for small Ω_b. So for the multidimensional model PCS we also fix $\Omega_b = 0.047$ and really use only 5 remaining parameters H_0, Ω_m, Ω_k, α, B. The value $\Omega_b = 0.047$ is fixed in all panels of Fig. 4 like for Fig. 3 (except for 3 bottom-right panels).

The dependence of $\min\chi^2_\Sigma = \min\limits_{\Omega_m,\Omega_k,\alpha,B}\chi^2_\Sigma$ on H_0 has the distinct minimum at $H_0 \simeq 69.52$ for $d = 1$ (the solid blue line here and in panels of this row). The similar behavior takes place for $d = 2$ (the violet dashed line) and for $d = 6$ (the purple dots). The minimal value $\min\chi^2_\Sigma \simeq 588.41$

for $d = 1$ is larger than for the ΛCDM and GCG models and for $d \geq 2$ the minima are still worse (see Table II).

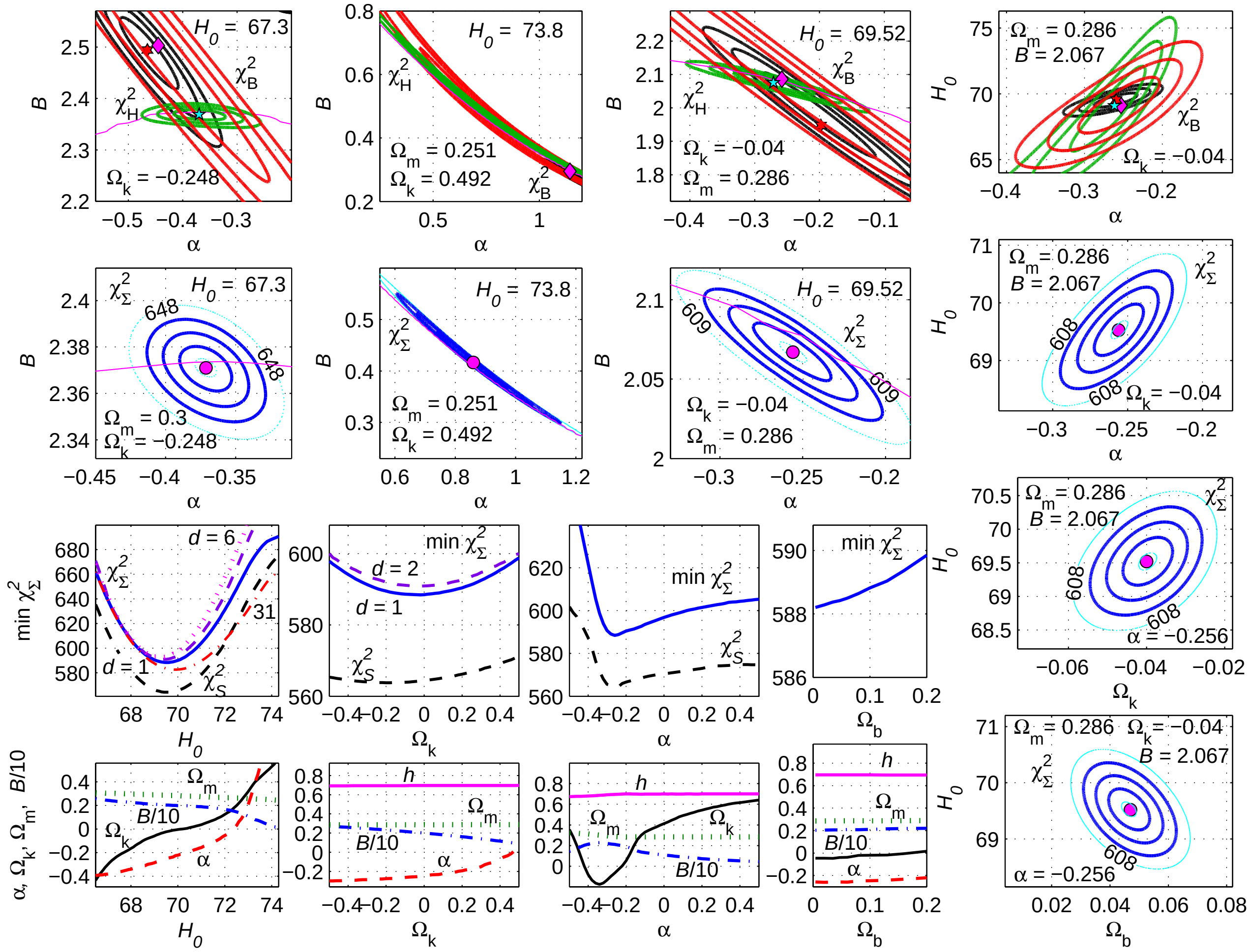

FIG. 4: The PCS model with $d = 1$. Notations and panels correspond to Fig. 3, in particular, in the bottom-left panels we analyze dependence of $\min \chi^2_\Sigma$ and parameters of a minimum point on H_0, Ω_k, α and Ω_b.

These bad results for the PCS model are connected with description of the $H(z)$ recent data with high z ($z > 2$ in Table VI). When we excluded 3 data points [14, 19, 20] for $H(z)$ with $z \geq 2.3$, we obtained absolutely other results presented below in Table IV.

In Fig. 4 all level lines and graphs correspond to the whole $H(z)$ data with $N_H = 34$ points. But only one except is done for the dependence of $\min \chi^2_\Sigma$ on H_0 for $d = 1$: here $N_H = 31$, this graph is shown as the red dash-and-dot line. The minimum value for this line $\min \chi^2_\Sigma \simeq 582.68$ is in Table IV.

Level lines of functions χ^2 are shown in Fig. 4 in the same panels as for the GCG model in Fig. 3, in particular, for the values (37) $H_0 = 67.3$, 73.8 and the optimal value $69.52\ \mathrm{km\,c^{-1}Mpc^{-1}}$. If H_0 is too large, the domain of acceptable level of χ^2_Σ becomes very narrow. One should note that for all level lines we change only two parameters, all remaining model parameters are fixed (they are from Table II or optimal for a given H_0).

In 6 top-left panels with the α, B plane we draw thin purple lines bounding the domain of regular solutions (below these lines). The upper domain (for larger B) consists of singular solutions, they have singularities in the past with infinite value of density ρ corresponding to nonzero value of the scale factor a [47]. These solutions are nonphysical and should be excluded. It is interesting that the optimal solutions in Fig. 4 and in Tables II and IV are near this border, but they are regular and describe the standard Big Bang $\rho \to \infty \ \Leftrightarrow \ a \to 0$ with dynamical compactification of extra dimensions.

IV. CONCLUSION

We considered how the ΛCDM, GCG and PCS models describe the observational data for type Ia supernovae, BAO and $H(z)$ [3], Tables V, VI. These observations distinctly restrict acceptable values for the Hubble constant H_0 and other parameters of the mentioned models. We used our calculations for dependance $\min\chi^2_\Sigma(p)$, where the absolute minimum (over other parameters) of the value (35) χ^2_Σ depend on a fixed parameter p. On the base of these calculations (presented partially in Figs. 2, 3, 4) we obtained the following 1σ estimates for parameters of the ΛCDM, GCG and PCS ($d = 1$) models:

TABLE III: 1σ estimates of model parameters ($\Omega_b = 0.047$ in the GCG and PCS models).

Model	$\min\chi^2_\Sigma$	H_0	Ω_k	other parameters
ΛCDM	585.35	70.262 ± 0.319	-0.04 ± 0.032	$\Omega_m = 0.276^{+0.009}_{-0.008}$, $\Omega_\Lambda = 0.769 \pm 0.029$
GCG	584.54	70.093 ± 0.369	-0.019 ± 0.045	$\alpha = -0.066^{+0.072}_{-0.074}$, $B_s = 0.759^{+0.015}_{-0.016}$
PCS, $d = 1$	588.41	$69.523^{+0.366}_{-0.350}$	-0.04 ± 0.045	$\Omega_m = 0.286 \pm 0.010$, $\alpha = -0.256^{+0.032}_{-0.03}$

Our estimates for the ΛCDM model are in agreement with the WMAP observational restrictions (38) on Ω_m, Ω_Λ, Ω_k [5], but they are in tension with the Planck data [8]. This fact is connected with too low value $H_0 = 67.3$ km c^{-1}Mpc^{-1} (37) in the Planck survey [8].

For the GCG model $\min\chi^2_\Sigma$ is slightly better and our limitations on H_0 and Ω_k in Table III are rather close to the ΛCDM case. However, if we require $\alpha \geq 0$ in accordance with Eq. (41) and Refs. [36, 37], the GCG model with the optimal value $\alpha = 0$ will be reduced to the ΛCDM model with its optimal parameters in Tables II, III and the same $\min\chi^2_\Sigma$.

Values χ^2_B and χ^2_Σ for the GCG model essentially depend on the expression for Ω_m^{eff} (39) or (40). But the optimal parameters in Table II for these expressions are rather close.

We mentioned above that the multidimensional model PCS is less effective in description of the considered observational data, and that the main problem of this model is connected with the $H(z)$ recent data with high z ($z > 2$). We excluded 3 $H(z)$ data points [14, 19, 20] with $z = 2.3$, 2.34, 2.36 and for remaining $N_H = 31$ points of $H(z)$ and the same SN and BAO data from [3], Table V. we calculated $\min\chi^2_\Sigma$ and optimal values of model parameters presented here in Table IV.

TABLE IV: Optimal values of model parameters for $\Omega_b = 0.047$ and $N_H = 31$ $H(z)$ data points with $z < 2$.

Model	$\min\chi^2_\Sigma$	H_0	Ω_m	other parameters
ΛCDM	583.71	70.12	0.281	$\Omega_\Lambda = 0.751$, $\Omega_k = -0.032$
GCG	583.70	70.11	0.291	$\Omega_k = -0.046$, $\alpha = -0.028$, $B_s = 0.756$
PCS, $d = 1$	582.68	69.89	0.281	$\Omega_k = -0.114$, $\alpha = -0.174$, $B = 2.078$
PCS, $d = 2$	582.93	69.82	0.282	$\Omega_k = -0.118$, $\alpha = -0.290$, $B = 1.616$
PCS, $d = 6$	583.23	69.78	0.282	$\Omega_k = -0.126$, $\alpha = -0.398$, $B = 1.291$

We see that the model PCS [46] describes the reduced set of data with $z < 2$ better than other models. The best fit is for $d = 1$, the optimal value of H_0 close to 70 $\mathrm{km\,c^{-1}Mpc^{-1}}$.

This example demonstrates that predictions of any cosmological model essentially depend on data selection. Moreover, there is the important problem of model dependence (in addition to mutual dependence) of observational data, in particular, data in Tables V, VI.

Leaving the last problem beyond this paper, we can conclude that the considered observations of type Ia supernovae [3], BAO (Table V) and the Hubble parameter $H(z)$ (Table VI) confirm effectiveness of the ΛCDM model, but they do not deny other models. The important argument in favor of the ΛCDM model is its small number N_p of model parameters (degrees of freedom). This number is part of information criteria of model selection statistics, in particular, the Akaike information criterion is [52] $AIC = \min\chi^2_\Sigma + 2N_p$. This criterion supports the leading position of the ΛCDM model.

Appendix A: Appendix

TABLE V: Values of $d_z(z) = r_s(z_d)/D_V(z)$ (31) and $A(z)$ (32) with corresponding errors [5, 21, 22]

z	$d_z(z)$	σ_d	$A(z)$	σ_A	Refs
0.106	0.336	0.015	0.526	0.028	[5]
0.20	0.1905	0.0061	0.488	0.016	[5]
0.35	0.1097	0.0036	0.484	0.016	[5]
0.44	0.0916	0.0071	0.474	0.034	[21]
0.57	0.07315	0.0012	0.436	0.017	[5, 22]
0.60	0.0726	0.0034	0.442	0.020	[21]
0.73	0.0592	0.0032	0.424	0.021	[21]

Measurements of $d_z(z)$ and $A(z)$ in Ref. [21] are not independent, they are described with the following elements of covariance matrices $C_d^{-1} = ||c^d_{ij}||$ and $C_A^{-1} = ||c^A_{ij}||$ in Eq. (34) [5, 21]:

$$\begin{array}{lll}
c^d_{44} = 24532.1, & c^d_{46} = -25137.7, & c^d_{47} = 12099.1,\\
c^d_{66} = 134598.4, & c^d_{67} = -64783.9, & c^d_{77} = 128837.6;\\
c^A_{44} = 1040.3, & c^A_{46} = -807.5, & c^A_{47} = 336.8,\\
c^A_{66} = 3720.3, & c^A_{67} = -1551.9, & c^A_{77} = 2914.9.
\end{array}$$

These matrices are symmetric ones, their remaining elements are $c_{ii} = 1/\sigma_i^2$, $c_{ij} = 0$, $i \neq j$.

Acknowledgments

G.S. would like to acknowledge the support of the Ministry of education and science of Russia (grant No. 1.476.2011).

[1] A.G. Riess et al., *Observational Evidence from Supernovae for an Accelerating Universe and a Cosmological Constant*, *Astron. J.* **116** (1998) 1009 [astro-ph/9805201].

TABLE VI: Values of the Hubble parameter $H(z)$ with errors σ_H from Refs. [9–20]

z	$H(z)$	σ_H	Refs	z	$H(z)$	σ_H	Refs
0.070	69	19.6	[13]	0.57	92.9	7.855	[17]
0.090	69	12	[9]	0.593	104	13	[11]
0.120	68.6	26.2	[13]	0.600	87.9	6.1	[12]
0.170	83	8	[9]	0.680	92	8;	[11]
0.179	75	4	[11]	0.730	97.3	7.0	[12]
0.199	75	5	[11]	0.781	105	12	[11]
0.200	72.9	29.6	[13]	0.875	125	17	[11]
0.240	79.69	2.65	[16]	0.880	90	40	[10]
0.270	77	14	[9]	0.900	117	23	[9]
0.280	88.8	36.6	[13]	1.037	154	20	[11]
0.300	81.7	6.22	[18]	1.300	168	17	[9]
0.350	82.7	8.4	[15]	1.430	177	18	[9]
0.352	83	14	[11]	1.530	140	14	[9]
0.400	95	17	[9]	1.750	202	40	[9]
0.430	86.45	3.68	[16]	2.300	224	8	[14]
0.440	82.6	7.8	[12]	2.340	222	7	[19]
0.480	97	62	[10]	2.360	226	8	[20]

[2] S. Perlmutter et al., *Measurements of Omega and Lambda from 42 high redshift supernovae*, *Astrophys. J.* **517** (1999) 565 [astro-ph/9812133].

[3] N. Suzuki et al., *The Hubble Space Telescope Cluster Supernova Survey: V. Improving the Dark Energy Constraints Above z¿1 and Building an Early-Type-Hosted Supernova Sample*, *Astrophys. J.* **746** (2012) 85 [arXiv:1105.3470].

[4] D.H. Weinberg et al., *Observational Probes of Cosmic Acceleration*, *Physics Reports* **530** (2013) 87 [arXiv:1201.2434].

[5] G. Hinshaw et al., *Nine-year Wilkinson Microwave Anisotropy Probe (WMAP) Observations: Cosmological Parameters Results*, *Astrophysical Journal Suppl.* **208** (2013) 19 [arXiv:1212.5226].

[6] D.J. Eisenstein et al., *Detection of the baryon acoustic peak in the large-scale correlation function of SDSS luminous red galaxies*, *Astrophys. J.* **633(2)** (2005) 560 [astro-ph/0501171].

[7] B.A. Reid et al., *Cosmological constraints from the clustering of the Sloan Digital Sky Survey DR7 luminous red galaxies*, *Mon. Not. Roy. Astron. Soc.* **404** (2010) 60 [arXiv:0907.1659].

[8] P.A.R. Ade et al., *Planck 2013 results. XVI. Cosmological parameters*, arXiv:1303.5076.

[9] J. Simon, L. Verde and R. Jimenez, *Constraints on the redshift dependence of the dark energy potential*, *Phys. Rev.* **D 71** (2005) 123001 [astro-ph/0412269].

[10] D. Stern, R. Jimenez, L. Verde, M. Kamionkowski and S. A. Stanford, *Cosmic chronometers: constraining the equation of state of dark energy. I: H(z) measurements*, *J. of Cosmology and Astropart. Phys.* **02** (2010) 008 [arXiv:0907.3149].

[11] M. Moresco et al., *Improved constraints on the expansion rate of the Universe up to z 1.1 from the spectroscopic evolution of cosmic chronometers*, *J. of Cosmology and Astropart. Phys.* **8** (2012) 006 [arXiv:1201.3609].

[12] C. Blake et al., *The WiggleZ Dark Energy Survey: Joint measurements of the expansion and growth history at* $z < 1$, *Mon. Not. Roy. Astron. Soc.* **425(1)** (2012) 405 [arXiv:1204.3674].

[13] C. Zhang et al., *Four New Observational H(z) Data From Luminous Red Galaxies Sloan Digital Sky Survey Data Release Seven*, arXiv:1207.4541.

[14] N.G. Busca et al., *Baryon Acoustic Oscillations in the Lyα forest of BOSS quasars*, *Astron. and Astrop.* **552** (2013) A96 [arXiv:1211.2616].

[15] C.H. Chuang and Y. Wang, *Modeling the Anisotropic Two-Point Galaxy Correlation Function on Small Scales and Improved Measurements of $H(z)$, $D_A(z)$, and $f(z)\sigma_8(z)$ from the Sloan Digital Sky Survey DR7 Luminous Red Galaxies*, *Mon. Not. Roy. Astron. Soc.* **435(1)** (2013) 255 [arXiv:1209.0210].

[16] E. Gaztañaga, A. Cabre, L. Hui, *Clustering of Luminous Red Galaxies IV: Baryon Acoustic Peak in the Line-of-Sight Direction and a Direct Measurement of $H(z)$*, *Mon. Not. Roy. Astron. Soc.* **399(3)** (2009) 1663 [arXiv:0807.3551].

[17] L. Anderson et al., *The clustering of galaxies in the SDSS-III Baryon Oscillation Spectroscopic Survey: Measuring D_A and H at $z = 0.57$ from the Baryon Acoustic Peak in the Data Release 9 Spectroscopic Galaxy Sample*, *Mon. Not. Roy. Astron. Soc.* **439(1)** (2014) 83 [arXiv:1303.4666].

[18] A. Oka et al., *Simultaneous constraints on the growth of structure and cosmic expansion from the multipole power spectra of the SDSS DR7 LRG sample*, *Mon. Not. Roy. Astron. Soc.* **439(3)** (2014) 2515 [arXiv:1310.2820].

[19] T. Delubac et al., *Baryon Acoustic Oscillations in the Lyα forest of BOSS DR11 quasars*, arXiv:1404.1801.

[20] A. Font-Ribera et al., *Quasar-Lyman α Forest Cross-Correlation from BOSS DR11: Baryon Acoustic Oscillations*, *J. of Cosmology and Astroparticle Phys.* **05** (2014) 027 [arXiv:1311.1767].

[21] C. Blake et al., *The WiggleZ dark energy survey: mapping the distance redshift relation with baryon acoustic oscillations*, *Mon. Not. Roy. Astron. Soc.* **418(3)** (2011) 1707 [arXiv:1108.2635].

[22] C-H. Chuang et al., *The clustering of galaxies in the SDSS-III Baryon Oscillation Spectroscopic Survey: single-probe measurements and the strong power of $f(z)\sigma_8(z)$ on constraining dark energy*, *Mon. Not. Roy. Astron. Soc.* **433(4)** (2013) 3559 [arXiv:1303.4486].

[23] T. Clifton, P.G. Ferreira, A. Padilla and C. Skordis, *Modified Gravity and Cosmology*, *Physics Reports* **513** (2012) 1 [arXiv:1106.2476].

[24] K. Bamba, S. Capozziello, S. Nojiri and S.D. Odintsov, *Dark energy cosmology: the equivalent description via different theoretical models and cosmography tests*, *Astrophys. and Space Science* **342** (2012) 155 [arXiv:1205.3421].

[25] E.J. Copeland, M. Sami and S. Tsujikawa, *Dynamics of dark energy*, *Int. J. Mod. Phys.* **D 15** (2006) 1753 [hep-th/0603057].

[26] M. Kunz, *The phenomenological approach to modeling the dark energy*, *Comptes rendus - Physique* **13** (2012) 539, [arXiv:1204.5482].

[27] T.P. Sotiriou and V. Faraoni, *f(R) theories of gravity*, *Rev. of Modern Phys.* **82** (2010) 451 [arXiv:0805.1726].

[28] S. Nojiri and S. D. Odintsov, *Unified cosmic history in modified gravity: from F(R) theory to Lorentz non-invariant models*, *Phys. Rept.* **505** (2011) 59 [arXiv:1011.0544].

[29] R. R. Caldwell, R. Dave and P. J. Steinhardt, *Cosmological imprint of an energy component with general equation of state*, *Phys. Rev. Lett.* **80** (1998) 1582 [astro-ph/9708069].

[30] J. Khoury and A. Weltman, *Chameleon cosmology*, *Phys. Rev.* **D 69** (2004) 044026 [astro-ph/0309411].

[31] A.Y. Kamenshchik, U. Moschella and V. Pasquier *An alternative to quintessence*, *Phys. Lett.* **B 511(2-4)** (2001) 265 [arXiv:gr-qc/0103004].

[32] M.C. Bento, O. Bertolami and A.A. Sen, *Generalized Chaplygin gas, accelerated expansion, and dark-energy-matter unification*, Phys. Rev. **D 66(4)** (2002) 043507 [arXiv:gr-qc/0202064].

[33] M. Makler, S.Q. de Oliveira and I. Waga, *Constraints on the generalized Chaplygin gas from supernovae observations*, *Phys. Lett.* **B 555(1-2)** (2003) 1 [arXiv:astro-ph/0209486].

[34] J. Lu, Y. Gui and L. Xu, *Observational constraint on generalized Chaplygin gas model*, *Eur. Phys. J. C.* **63** (2009) 349 [arXiv:1004.3365].

[35] N. Liang, L. Xu and Z. Zhu, *Constraints on the generalized Chaplygin gas model including gamma-ray bursts via a Markov Chain Monte Carlo approach*, *Astron. Astrophys.* **527** (2011) A11 [arXiv:1009.6059].

[36] J.P. Campos, J.C. Fabris, R. Perez, O.F. Piattella and H. Velten, *Does Chaplygin gas have salvation? Eur. Phys. J. C.* **73** (2013) 2357 [arXiv:1212.4136].

[37] L. Xu, J. Lu and Y. Wang, *Revisiting Generalized Chaplygin Gas as a Unified Dark Matter and Dark Energy Model*, *Eur. Phys. J. C.* **72** (2012) 1883 [arXiv:1204.4798].

[38] J. Lu, L. Xu, Y. Wu, and M. Liu, *Combined constraints on modified Chaplygin gas model from cosmological observed data: Markov Chain Monte Carlo approach*, *Gen. Rel. Grav.* **43** (2011) 819 [arXiv:1105.1870].

[39] B.C. Paul and P. Thakur, *Observational constraints on modified Chaplygin gas from cosmic growth*, *J.*

of Cosmology and Astropart. Phys. **11** (2013) 052 [arXiv:1306.4808].

[40] N. Mohammedi, *Dynamical Compactification, Standard Cosmology and the Accelerating Universe*, *Phys. Rev.***D 65** (2002) 104018 [hep-th/0202119].

[41] F. Darabi, *Accelerating Universe and Dynamical Compactification of Extra Dimensions*, *Class. Quant. Grav.* **20** (2003) 3385 [gr-qc/0301075].

[42] T. Bringmann, M. Eriksson and M. Gustafsson, *Cosmological Evolution of Homogeneous Universal Extra Dimensions*, *Phys. Rev.* **D 68** (2003) 063516 [astro-ph/0303497].

[43] D. Panigrahi, Y.Z. Zhang and S. Chatterjee, *Accelerating Universe as Window for Extra Dimensions*, *Int. J. Mod. Phys.* **A 21** (2006) 6491 [gr-qc/0604079].

[44] C. A. Middleton and E. Stanley, *Anisotropic evolution of 5D Friedmann-Robertson-Walker spacetime*, *Phys. Rev.* **D 84** (2011) 085013 [arXiv:1107.1828].

[45] H. Farajollahi and H. Amiri, *5D noncompact Kaluza -Klein cosmology in the presence of Null perfect fluid*, *Int. J. Mod. Phys.* **D 19** (2010) 1823 [arXiv:1005.3140].

[46] I. Pahwa, D. Choudhury and T. R. Seshadri, *Late-time acceleration in Higher Dimensional Cosmology*, *J. of Cosmology and Astroparticle Phys.* **09** (2011) 015 [arXiv:1104.1925].

[47] O.A. Grigorieva and G.S. Sharov, *Multidimensional gravitational model with anisotropic pressure*, *Intern. Journal of Modern Physics* **D 22** (2013) 1350075 [arXiv:1211.4992].

[48] A.G. Riess et al., *A 3% Solution: Determination of the Hubble Constant with the Hubble Space Telescope and Wide Field Camera 3*, *Astrophys. J.* **730(2)** (2011) 119 [arXiv:1103.2976].

[49] et al. 2003, ApJ, 594, 1 J.L. Tonry et al., *Cosmological Results from High-z Supernovae*, *Astrophys. J.* **594** (2003) 1, arXiv:astro-ph/0305008

[50] . R.A. Knop et al., *New Constraints on Ω_m, Ω_Λ, and w from an Independent Set of Eleven High-Redshift Supernovae Observed with HST1*, *Astrophys. J.* **598** (2003) 102, arXiv:astro-ph/0309368.

[51] M. Kowalski et al., *Improved cosmological constraints from new, old and combined supernova datasets*, *Astrophys. J.* **686** (2008) 749 [arXiv:0804.4142].

[52] K. Shi, Y.F. Huang and T. Lu, *A comprehensive comparison of cosmological models from the latest observational data*, *Monthly Notices Roy. Astronom. Soc.* **426** (2012) 2452 [arXiv:1207.5875].

[53] O. Farooq, D. Mania and B. Ratra, *Hubble parameter measurement constraints on dark energy*, *Astrophys. J.* **764** (2013) 139 [arXiv:1211.4253].

[54] O. Farooq and B. Ratra, *Hubble parameter measurement constraints on the cosmological deceleration-acceleration transition redshift*, *Astrophys. J.* **766** (2013) L7, [arXiv:1301.5243].

[55] O. Farooq, *Ph.D. thesis*, arXiv:1309.3710.

[56] J.R. Gott III, M.S. Vogeley, S. Podariu and B. Ratra, *Median statistics, h0, and the accelerating universe*, *Astrophys. J.* **549** (2001) 1.